Since January 2020 Elsevier has created a COVID-19 resource centre with free information in English and Mandarin on the novel coronavirus COVID-19. The COVID-19 resource centre is hosted on Elsevier Connect, the company's public news and information website.

Urban Forestry & Urban Greening 62 (2021) 127126

Contents lists available at ScienceDirect

Urban Forestry & Urban Greening

journal homepage: www.elsevier.com/locate/ufug

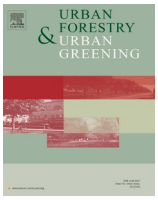

Using urban landscape pattern to understand and evaluate infectious disease risk

Yang Ye [a,b], Hongfei Qiu [a,b,*]

[a] Department of Landscape Architecture, College of Horticulture and Forest, Huazhong Agricultural University, No. 1, Shizishan Street, Hongshan District, Wuhan, Hubei Province, 430070, China
[b] Key Laboratory of Urban Agriculture in Central China, Ministry of Agriculture and Rural Affairs, China

ARTICLE INFO

Handling Editor: Wendy Chen

Keywords:
COVID-19
Infection risk
Landscape epidemiology
Landscape metrics
Landscape pattern
Wuhan

ABSTRACT

COVID-19 case numbers in 161 sub-districts of Wuhan were investigated based on landscape epidemiology, and their landscape metrics were calculated based on land use/land cover (LULC). Initially, a mediation model verified a partially mediated population role in the relationship between landscape pattern and infection number. Adjusted incidence rate (AIR) and community safety index (CSI), two indicators for infection risk in sub-districts, were 25.82~63.56 ‰ and 3.00~15.87 respectively, and central urban sub-districts were at higher infection risk. Geographically weighted regression (GWR) performed better than OLS regression with AICc differences of 7.951~181.261. The adjusted R^2 in GWR models of class-level index and infection risk were 0.697 to 0.817, while for the landscape-level index they were 0.668 to 0.835. Secondly, 16 key landscape metrics were identified based on GWR, and then a prediction model for infection risk in sub-districts and communities was developed. Using principal component analysis (PCA), development intensity, landscape level, and urban blue-green space were considered to be principal components affecting disease infection risk, explaining 73.1 % of the total variance. Cropland (PLAND and LSI), urban land (NP, LPI, and LSI) and unused land (NP) represent development intensity, greatly affecting infection risk in urban areas. Landscape level CONTAG, DIVISION, SHDI, and SHEI represent mobility and connectivity, having a profound impact on infection risk in both urban and suburban areas. Water (PLAND, NP, LPI, and LSI) and woodland (NP, and LSI) represent urban blue-green spaces, and were particularly important for infection risk in suburban areas.

Based on urban landscape pattern, we proposed a framework to understand and evaluate infection risk. These findings provide a basis for risk evaluation and policy-making of urban infectious disease, which is significant for community management and urban planning for infectious disease worldwide.

1. Introduction

Landscape epidemiology is a multi-functional concept, on which the occurrence and spread of disease is a function of people, place, and time (Emmanuel et al., 2011). From a potential public health risk perspective, disease vectors, hosts, and pathogens are often associated with landscapes that affect the distribution and abundance of ecological determinants in the environment (Ostfeld et al., 2005). Urbanization has led to more than 56 % of the world's population living in cities, but it has also made infectious disease risk rise sharply in cities (Hamidi et al., 2020). According to the UN-Habitat, cities (with 95 % cases) are COVID-19 outbreak centers, especially in unplanned and naturally formed residential areas (UN-HABITAT, 2020). Therefore, there is an urgent need for a framework to understand and evaluate infection risk in cities based on landscape epidemiology, which is significant for urban planning and infectious disease prevention.

Landscape epidemiology generally recognizes that landscape pattern is an important infectious disease driving factor, especially in cities. Some evidence indicates that human changes in the natural landscape promote tuberculosis spread in cities (Webster, 2020). Infection risk of Avian influenza and malaria in Egypt (Young et al., 2017) is also related to landscape pattern (Abdelsattar and Hassan, 2020). Relevant studies have confirmed the close relationship between landscape composition and structure, such as forest fragmentation, and infectious disease risk

* Corresponding author at: Department of Landscape Architecture, College of Horticulture and Forest, Huazhong Agricultural University, Hongshan District, Wuhan, 430070, China.
E-mail addresses: albertwilliams@foxmail.com (Y. Ye), qiuhongfei@mail.hzau.edu.cn (H. Qiu).

https://doi.org/10.1016/j.ufug.2021.127126
Received 10 June 2020; Received in revised form 26 February 2021; Accepted 30 March 2021
Available online 2 April 2021

(Messier et al., 2015). Often, research has focused on a single urban landscape component, such as green space at class level (Messier et al., 2015), and claimed that detailed spatial patterns of different landscape characteristics (such as shape, configuration, evenness, fragmentation, clustering, and edge effect) should be quantified in future surveys on infection risk (Hoek et al., 2008). From a landscape climate perspective, Halimi et al. (2014) developed a predictive model of malaria incidence rate and typhoid fever prevalence in different regions of Iran and considered that non-landscape factors such as social economy, lifestyle, and neighborhood relationships required further consideration. Until now, COVID-19 has been studied and related to urban blue-green spaces, although more evidence at the sub-district and community scale in cities needs to be added. For example, temperature differences between cities affect the distribution of case numbers (Zhu and Xie, 2020), and there is evidence that Wuhan COVID-19 mortality is affected by temperature and humidity (Ma et al., 2020). Moreover, some studies have shown that COVID-19 exhibits differences in geographical spatial distribution, and that more fine-grained spatial distribution research is needed (Zhou et al., 2020). Presently, remote sensing technology has been widely used to describe landscape patterns (Hoyle et al., 2017). Calculated from land use/land cover (LULC), landscape metrics quantify spatial heterogeneity in terms of composition (i.e. what exists – quantity and diversity of patches) and configuration e.g., spatial arrangement, patch shape, and aggregation (Dramstad et al., 2006), and link landscape pattern with biodiversity, hydrological process, environment and human health (Uuemaa et al., 2013). Therefore, data accessibility makes landscape pattern an ideal indicator of urban infection risk among various potential factors. Connolly et al. (2021) stress that it is difficult to clarify each specific factor affecting infection risk, but it is more important to propose a framework to evaluate infection risk in cities.

A general hypothesis in landscape epidemiology is that factors may affect infection number through population density (Hassan et al., 2021), especially in urban environments (Gao and Hethcote, 1992). Moreover, the current understanding of the effects of environmental and socio-economic factors on the COVID-19 incidence rate is rather limited (Hassan et al., 2021). Meanwhile, spatial heterogeneity is a common focus in landscape epidemiology. For example, studies used geographically weighted regression (GWR) to explore the tuberculosis epidemic (W. Wang et al., 2016) and hand, foot, and mouth disease (Hu et al., 2020). Their findings suggest that local regression techniques provide an understanding of how landscape pattern affect infection risk in city urban and suburban areas. However, population density and spatial heterogeneity are rarely discussed in studies on landscape epidemiology involving urban infectious disease risk. Meanwhile, key landscape metrics have not been systematically determined, creating obstacles to understanding and evaluating infection risk in cities.

Based on the relationship between landscape pattern and infection risk, our research objectives are to: 1) determine spatial heterogeneity of the relationship based on the mediating role of population density; and 2) identify principal components of key landscape metrics and then develop a prediction model to evaluate risk infection. Using urban landscape pattern to understand and evaluate infectious disease risk is significant for community management and urban planning for infection risk prevention worldwide.

2. Methodology

2.1. Study area

We selected the central China city of Wuhan as our study area. Wuhan is located at 113° 41′ - 115° 05′ E and 29° 58′ - 31° 22′ N, on a river/lake alluvial plain (Fig. 1). By the end of 2019, Wuhan covered 8569.15 square kilometers and had a registered population of 11.212 million (Ye and Qiu, 2021a). Under urban planning guidance (Fig. 1), Wuhan was formed as an open spatial layout structure of "main urban area as the core, multi axis and centers", with three urban sub-centers, six new towns, and six “large wedges” (urban blue-green space) (Ye and Qiu, 2021b). Municipal districts in China’s cities can be divided into

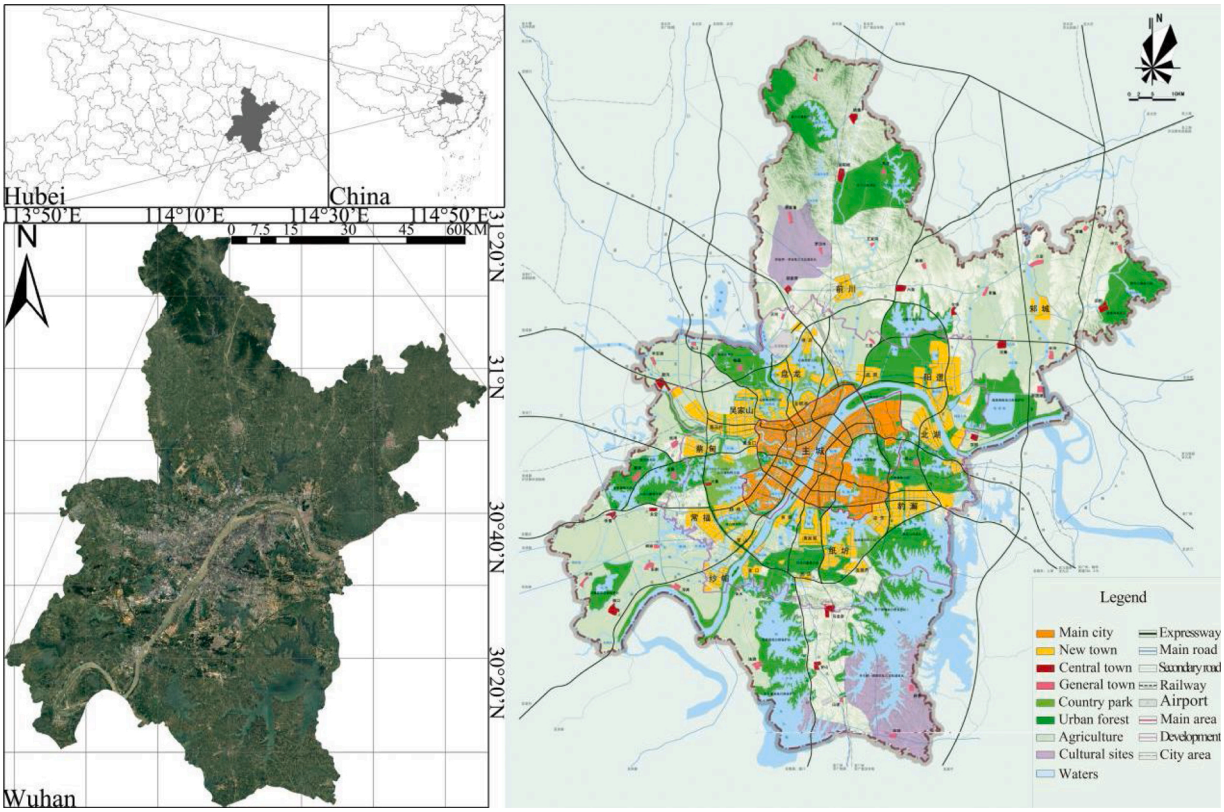

Fig. 1. Geographical position (left) and spatial layout plan (2006-2020) of study area (Wuhan, China).

urban and suburban districts (area) (K. Wang and Qi, 2017). Urban districts are the main urban area spaces, which are the political, economic, and cultural city centers, while suburban districts are the spaces with both urban and rural characteristics. Wuhan City has thirteen municipal districts (seven urban districts and six suburban districts), which can be further divided into 161 sub-districts (Fig. 2a) (Ye and Qiu, 2020). Detailed information on the Wuhan sub-districts can be found on the local government website (http://mzj.wuhan.gov.cn/). When COVID-19 was first discovered, Wuhan experienced a lockdown from January 23 to April 8, 2020. On April 24, 2020, the Wuhan Municipal Health Commission (WMHC) announced that Wuhan was a low-risk area in China and that novel coronavirus pneumonia had been cleared in Wuhan's hospital. The global spread of COVID-19 is concentrated in sub-districts and communities (Amariles et al., 2021), and thus we focused on the disease distribution in sub-districts up to May 8, 2020, as infection number and population data at the sub-district scale was available (unavailable for communities) (Ye et al., 2021).

2.2. Landscape pattern

2.2.1. Data source

To accurately describe the Wuhan landscape pattern, we obtained the 2019 Wuhan LULC, which used the Chinese national classification method and has a 30 m accuracy (Zhang et al., 2020b). The data set was obtained from the Data Center for Resources and Environmental Sciences, Chinese Academy of Sciences (RESDC) (http://www.resdc.cn) (Zhang et al., 2020b). It is the most accurate remote sensing monitoring database product for LULC in China and plays an important role in national land resource surveys and hydrological and ecological studies (Li et al., 2018). To facilitate calculation and discussion, we adopted the first level classification. Landscape classes are divided into: 1.Cropland, 2.Woodland, 3.Grassland, 4.Water, 5.Urban land, and 6.Unused land (Table 1). Compared with the high-density urban area in Wuhan, more than 70 % of the total land area (about 1100 square kilometers) is covered by mountainous vegetation and urban forests (Fig. 2). In the 21 st century, the Wuhan landscape pattern has changed considerably with urbanization (X. Wang et al., 2008). For instance, patch number and fragmentation degree of each wetland type has increased, and wetland area has decreased due to intensive past human activities (Ye and Qiu, 2021b). This had led to the fragmentation of natural wetlands and a reduction in their dominance.

2.2.2. Landscape metrics

The calculation of landscape metrics has been incorporated into satellite image-based landscape analysis. Established on the classic "patch corridor matrix" theory of landscape ecology, landscape metric is a highly quantifiable measure that has been widely used in landscape epidemiology research (Messier et al., 2015). Class- and landscape-level indices are typically computed for the entire landscape; i.e., they quantify the structure of the individual class or the entire mosaic over the full extent of the data. Class-level indices represent the amount and spatial distribution of a single patch type and are interpreted as the fragmentation index while landscape-level indices represent the spatial pattern of the entire landscape mosaic and are generally interpreted more broadly as the landscape heterogeneity index because they measure overall landscape structure (McGarigal, 2014). Because of similar diffusion patterns, we draw on the typical research paradigm of landscape ecology, especially the study of pollutant diffusion in the urban environment (Łowicki, 2019).

We selected eight landscape metrics (Abdelsattar and Hassan, 2020) according to the literature (Moon et al., 2019), and quantified the detailed landscape pattern in 161 sub-districts (Deilami et al., 2017) using landscape ecology knowledge (Bonnell et al., 2016). Among them, four class-level indices represent the number and spatial pattern of a specific landscape class (cropland, woodland, grassland, water, urban land, and unused land) in a sub-district, which can be related to urban landscape layout: Percentage of landscape classes (PLAND), Number of Patches (NP), Landscape Similarity Index (LSI), and Largest Patch Index (LPI). The four landscape-level indices assess the combination, arrangement, and mixture of all landscape classes which are closely related to city structure and shape. The widely used landscape-level indices we adopted to quantify landscape diversity are: Contagion Index (CONTAG), Landscape Division Index (DIVISION), Shannon's Diversity Index (SHDI), and Shannon's Evenness Index (SHEI). All

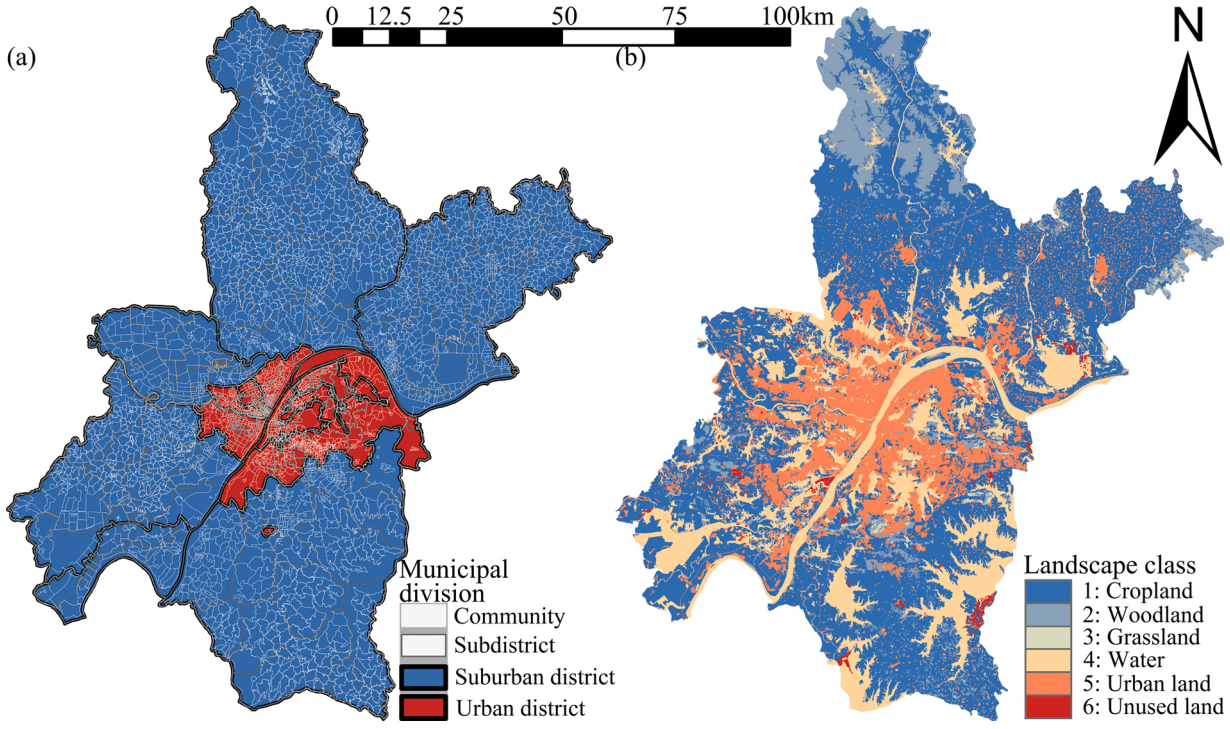

Fig. 2. Municipal division (a) and LULC (b) in Wuhan, China (2020).

Table 1
Categories of landscape class (land use/land cover) in Wuhan.

Landscape class	Landscape name	Content	Description
1	Cropland	11.Paddy field; 12.Dry land	The land where crops are planted, including mature cultivated land, newly opened wasteland, leisure land, rotation land, grassland, and rotation land; agricultural fruit, mulberry and forestry land mainly planted with crops; and beaches and beaches cultivated for more than three years
2	Woodland	21.Forest land; 22. Shrubwood; 23.Sparse woodland; 24.Other woodland	Forest land for trees, shrubs, bamboos, and coastal mangroves
3	Grassland	31.High coverage grassland; 32.Medium coverage grassland; 33. Low coverage grassland	All kinds of grasslands with mainly herbaceous plants and covering more than 5 %, including shrub/grassland dominated by animal husbandry and sparse forest grassland with canopy density less than 10 %
4	Water	41.Channel; 42.Lake; 43.Reservoir pond; 44. Permanent Glacial Snow; 45.Tidal flat; 46. Beach land	Land with natural water areas and water conservancy facilities
5	Urban land	51.City and town; 52. Rural settlement; 53. Other construction land	Industrial, mining, transportation and other lands outside the urban and rural residential areas and counties
6	Unused land	61.Sand; 62.Gobi; 63. Saline alkali soil; 64. Swamp land; 65.Bare land; 66.Bare rock gravel; 67.Otherland	Unused land, including difficult to use land

landscape metrics (Table S1) were calculated using Fragstats (version 4.2), a widely used program for spatial pattern analysis of categorical maps. The descriptive statistics and spatial distribution of landscape metrics are shown in Table 2 and Fig. 3 respectively.

2.3. Infection risk

2.3.1. Adjusted incidence rate

Infection risk is defined on a cross-sectional study, which is a classic landscape epidemiology method (Emmanuel et al., 2011). With the development of information technology, internet applications have been widely used in the study on urban infectious diseases (Schwab-Reese et al., 2018). Some researchers have used Twitter to construct an effective surveillance system based on tweets, indicating that disease outbreak risk can be forewarned with data generated by social media (Jain and Kumar, 2015). Similarly, Flusurvey, a community surveillance system for influenza-like illness, is used to conduct statistics on incidence rate. Researchers believe that internet-based data sources have created conditions for standardized and refined measurement of seasonal influenza and other respiratory infections in the UK and other areas of the world (Camacho et al., 2013). WeChat, the most popular social mobile app in China (Zhang et al., 2020a), is often used in population surveys and for geospatial location statistics in the urban environment (Ye and Qiu, 2021a). During the Wuhan COVID-19 outbreak, many residents spontaneously published case numbers for their sub-districts in WeChat. It should be noted that not all daily cases in each sub-district were uploaded to WeChat, so the data is a sample, rather than a thorough survey. The daily data were summed to obtain case numbers in all 161 sub-districts respectively. On May 8, 2020, Wuhan became a low-risk area of the epidemic in China, and the WMHC announced a cumulative report of 50,333 confirmed cases based on the current address, which was used for correction and test. As of May 8, 2020, the case number uploaded to WeChat was 6,250, so the calibration coefficient (r) is 8.053. The adjusted case numbers are the product of case numbers counted by WeChat and r. The adjusted case number in each sub-district was accumulated to obtain data for thirteen Wuhan districts, which is consistent with the data released by WMHC (Fig. 4a), (Kempen et al., 2019). To exclude the effect of population density (by hypothesis) on the results, the adjusted incidence rate (ARI, ‰) was calculated by:

$$\mathrm{AIR} = \frac{\mathrm{N_w} * \mathrm{r} * 10000}{\mathrm{P}} \quad (1)$$

Where, N_w is the case number counted by WeChat; r is the calibration coefficient (8.053, in this study); and P is the number of permanent residents. All of these quantities are at the sub-district scale.

2.3.2. Community safety index

Increasingly, studies have pointed out that it is inadequate to measure city infection risk using incidence rate only. Because many factors affect infection risk, urban spaces are similar to a chaotic body, suggesting that more abstract indicators are considered to be meaningful for

Table 2
Descriptive statistics of landscape metrics and infection risk (N = 161).

	Class-level index				Landscape-level index				Infection risk	
Landscape class	PLAND (%)	LSI	LPI(%)	NP (n)	CONTAG	DIVISION	SHDI	SHEI	AIR	CSI
1	29.075 ± 28.808	5.315 ± 4.604	20.793 ± 24.983	12.882 ± 17.843						
2	4.357 ± 10.317	2.702 ± 3.628	2.653 ± 7.914	8.603 ± 21.251						
3	2.230 ± 11.340	1.186 ± 1.788	1.995 ± 11.307	1.590 ± 3.403	58.255 ± 21.856	0.512 ± 0.297	0.7215 ± 0.399	0.517 ± 0.241	47.747 ± 11.900	10.797 ± 2.550
4	19.060 ± 18.627	4.640 ± 3.258	13.909 ± 17.129	12.721 ± 14.544						
5	44.812 ± 36.159	5.729 ± 4.543	39.222 ± 37.674	24.261 ± 40.503						
6	1.407 ± 8.960	1.235 ± 1.920	0.953 ± 7.666	2.093 ± 4.266						

Note: mean ± SD.

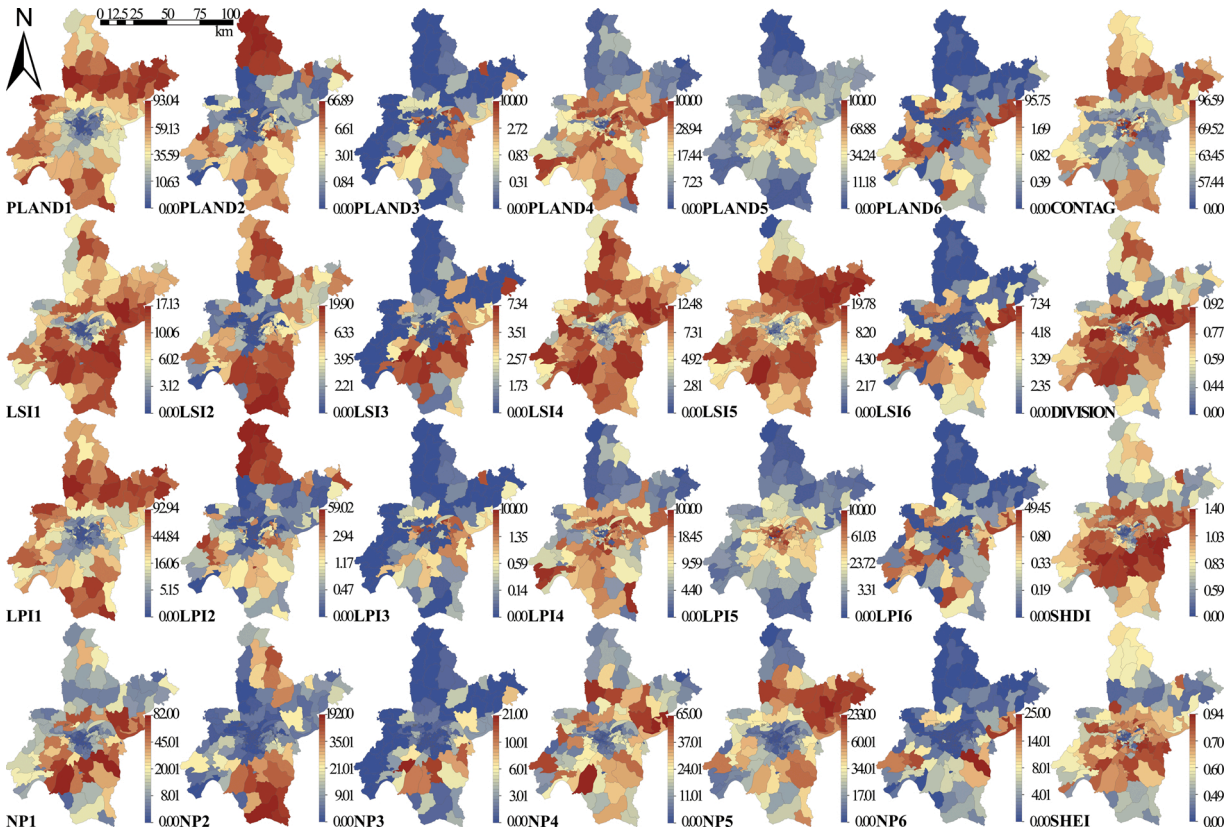

Fig. 3. Landscape metrics (class-level and landscape-level index) in subdistricts of Wuhan.

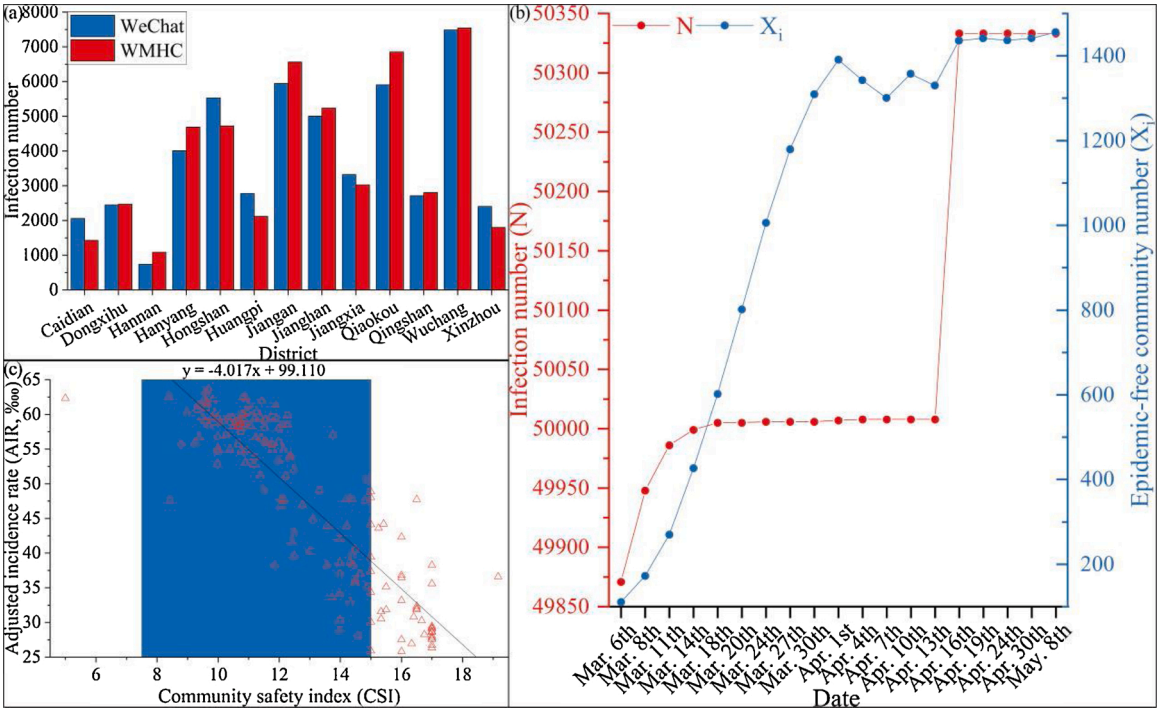

Fig. 4. Epidemiological cross-sectional statistics. (a) Infection number of COVID-19 in 13 Wuhan's districts (Until May 8, 2020), (b) Temporal variation of infection case and epidemic-free community number in Wuhan, and (c) Relationship between AIR and CSI.

the control and early warning of infectious diseases in cities (Vinarti and Hederman, 2019). From March 6 to May 8, 2020, WMHC publicized seventeen batches of epidemic-free communities to urgently identify infection risk in sub-districts. According to COVID-19 epidemiological characteristics, the most obvious selection criteria for epidemic-free communities is that they have suffered no infection for two weeks. For

detailed information, please see the WMHC website (http://wjw.wuhan.gov.cn/). Resulting from epidemic changes, some epidemic-free communities were canceled or suspended, so batch accumulation was used to calculate the number of epidemic-free communities. For a sub-district, the community safety index (CSI) is considered to be the proportion of epidemic-free communities in all communities, which was calculated by:

$$CSI = \frac{\sum_{i=1}^{n} X_i}{X} \quad (2)$$

Where, X_i is the number of epidemic-free communities in batch *i*, and *i* is from 1 to 17 in this study; and *X* is the total number of communities in a sub-district.

The descriptive statistic of infection risk is shown in Table 2. The number of cases (N) and epidemic-free communities (X_i) released by WMHC from March 6 to May 8, 2020, are shown in Fig. 4b. The abnormally high April 16 value was due to the inclusion of previously missed cases, and the fluctuation in the number of epidemic-free communities in April was due to the screening of asymptomatic infections in Wuhan. On March 14, new case numbers in Wuhan slowed down significantly, and the number of epidemic-free communities grew rapidly, indicating that the epidemic was basically under control. Therefore, it was considered reasonable for the local government to lift the city lockdown after a 25-day observation period. CSI can quickly reflect infection risk of epidemic diseases in a sub-district or community, so it is an important index to guide emergency decision-making for cities like Wuhan. To determine CSI effectiveness, we examined the relationship between CSI and AIR (traditional indicator) and found good consistency (Spearman R = -0.854, $p < 0.001$) at the sub-district scale as shown in Fig. 4c.

2.4. Data analysis

2.4.1. Mediation model

To avoid redundancy, preliminary multiple linear regression between infection number and landscape pattern was used to select the eight most relevant landscape metrics (four class-level and four landscape-level indices) for mediation detection. Population data in Wuhan's sub-districts were obtained from China's sixth population census, and after a spatial link by Arc GIS, the population density in sub-districts were calculated (Ye et al., 2021). In the mediation model, we treated population density as the mediator, eight selected landscape metrics as independent variables, and infection numbers as the dependent variable. The "model 4" in the PROCESS macro for SPSS was used to run the mediation model with 10,000 bootstrapping resamples adopted (Hayes, 2013).

2.4.2. GWR and prediction models

Because urban infection risk and landscape pattern generally show spatial heterogeneity (W. Wang et al., 2016), global regression (such as ordinary least squares, OLS) and local regression (such as GWR) were compared in this study. GWR 4.0 software was used to build models to explain infection risk with landscape metrics as predictors. Four groups of GWR models were built to examine the effects of landscape pattern on infection risk in 161 sub-districts, respectively (Table 3). Independent variables in Models 1 and 3 were four class-level indices, while they were four landscape-level indices in Models 2 and 4. The dependent variable in Models 1 and 2, was AIR, while it was CSI in Models 3 and 4. A series of key landscape metrics were identified by these GWR models, and then we used PCA to classify them into principal components to explain infection risk observed in sub-districts. Finally, we developed a prediction model to evaluate infection risk based on landscape pattern (Vizzari and Sigura, 2015). A comprehensive flow chart for this process can be seen in Fig. 5.

3. Results

3.1. Population mediation effects

The AIR in 161 Wuhan sub-districts was between 25.82 and 63.56 ‰, and the sub-districts with high AIR were concentrated in the city center (Fig. 6a). The CSI in 161 Wuhan sub-districts was between 3.00 and 15.87, and the CSI spatial distribution was still high in the middle and low around the periphery, but the patterns were not as striking as for AIR (Fig. 6b). We employed two approaches to test the mediating effects of population density. First, we adopted the bootstrap sampling method (bootstrap sample size = 5000) recommended by MacKinnon et al. (2004) to generate the asymmetric confidence intervals (CIs) for indirect relationships. Table 4 shows the mediating role of population density, and Table 5 reports detailed mediating effects. At class level, population density mediated the relationship between PLAND1, LPI5 and infection number because their CIs did not include zero; by contrast, population density cannot mediate the relationship between LSI2, PLAND4 and infection number, because the CIs contained zero. At a landscape level, the mediating effects of population density on CONTAG, DIVISION, SHEI, and infection number were supported, with CIs of the same sign; however, the 95 % CI of its mediating effect on SHDI and infection number was (−0.11, 0.50), which included zero. These show that cropland and urban land are more suitable expressions of infection risk caused by population density.

We used the method suggested by Baron and Kenny (1986) to test whether the supported mediating effects were full or partial. If the relationship between the independent and dependent variables controlled by the mediator is insignificant, the relationship is fully mediated; otherwise, it is partially mediated. Table 5 shows the results of the Baron and Kenny (1986) mediation test, and are consistent with those of the bootstrapping mediation test, indicating the robustness of the hypothesis testing. For mediation degree, the mediating effects hypothesized in class level (PLAND1 and LPI5) were full mediation, and landscape level mediating effects (CONTAG, DIVISION, and SHEI) were

Table 3
Variables of OLS and GWR models.

Category	Variable/method	Model 1−1	Model 1−2	Model 2−1	Model 2−2	Model 3−1	Model 3−2	Model 4−1	Model 4−2
Class level	PLAND								
	LSI	√		√					
	LPI								
	NP								
Landscape level	CONTAG								
	DIVISION					√		√	
	SHDI								
	SHEI								
Infection risk	AIR	√				√			
	CSI			√				√	
Regression technique	Global	√		√		√		√	
	Local		√		√		√		√

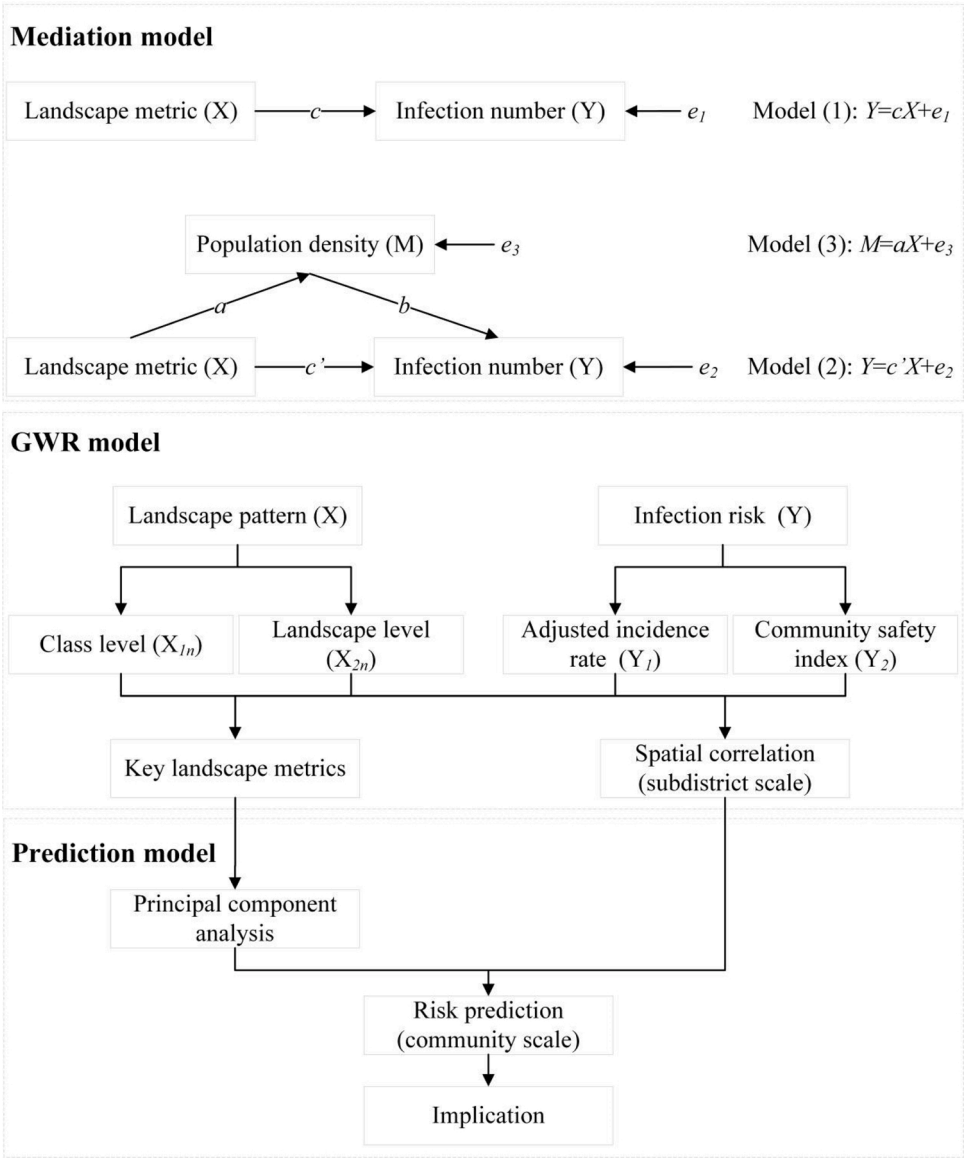

Fig. 5. Comprehensive flow chart of mediation, GWR, and prediction models.

partial mediation. This indicates that landscape-level index reflects the impact of other potential mediators on infection risk. Results prove the previous hypothesis that population density mediates the impact of landscape pattern on infection number. Therefore, it is more appropriate to use infection rate and community safety rather than infect number to represent infection risk.

3.2. *Geographically weighted regression*

To address spatial features, the OLS regression model was performed and results were compared with those from the GWR model. Meanwhile, a geographical variability test was conducted to examine spatial heterogeneity. Due to the unbalanced outcome distribution of the OLS regression, adaptive Gaussian was considered as the kernel type. Bandwidth selection method followed the golden section search of software GWR4, and best bandwidth value was 57.65~161.00 nearest neighbors (Table 6). In terms of goodness-of-fit, Table 6 summarizes the interpretation effects of the OLS and GWR models. GWR models reduced residual sum of squares (RSS) and the sigma estimate by 36.51 ~ 11083.92 and 0.05 ~ 4.88, respectively, indicating that the GWR model was more suitable for infection risk expatiation. The Geographical variability test was examined by model comparison, and the model with a lower AICc value (difference > 3) would be regarded as the better model. The GWR models AICc value decreased by 7.951~181.261 (except for Model 2-2), which therefore illustrates that GWR models perform better than OLS regression models.

Fig. 7 shows the spatial distribution of standard residuals in GWR models. The sub-districts with standard residual absolute values of more than 2.5 may have local multicollinearity problems. The problem was only found in a metallurgical base sub-district in Wuhan, which is relatively independent and with weak externality (Fig. 7). Namely, GWR models have good applicability for most sub-districts. Fig. 8 shows the spatial distribution of local R^2 in GWR models. Models 1 and 2 with class-level indices (local $R^2 = 0.71 \sim 0.86$) were more stable than Models 3 and 4 with landscape-level indices (local $R^2 = 0.08 \sim 0.92$). Meanwhile, local R^2 in suburban sub-districts was significantly higher than that in urban sub-districts, which indicates that the landscape pattern is better for infection risk evaluation in areas with lower urbanization. These findings confirm the mediating role of population density on infection number.

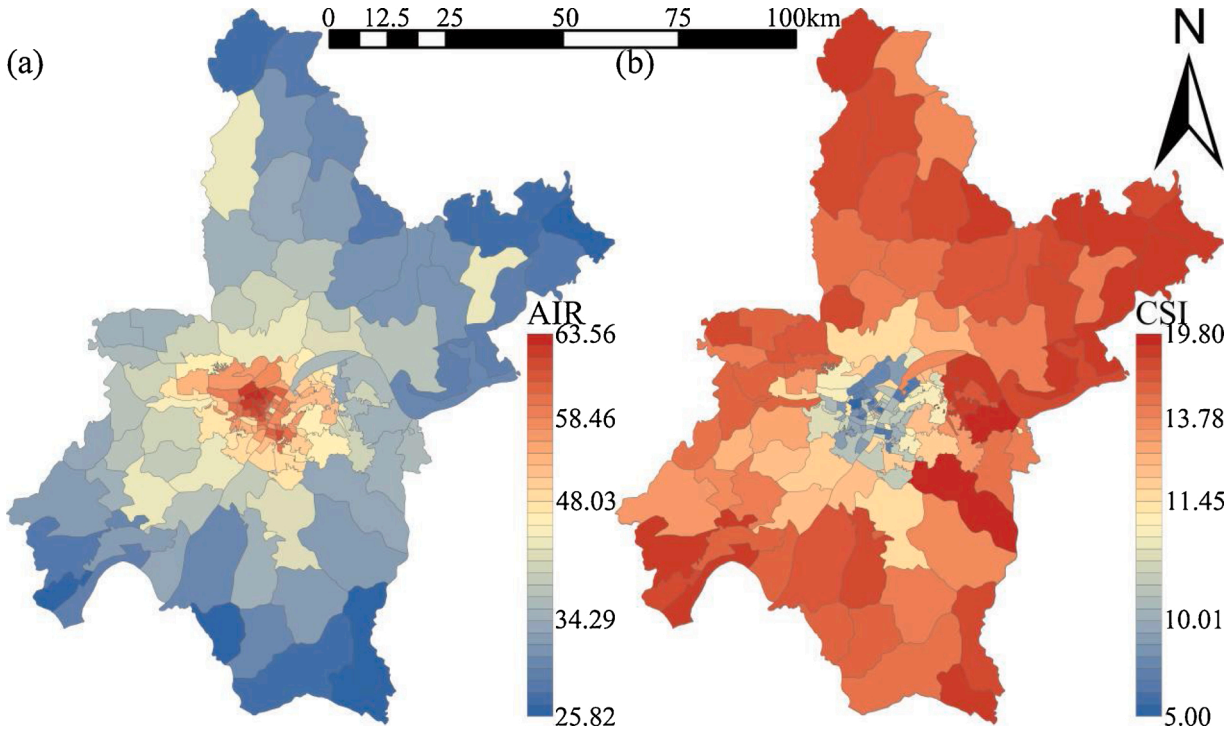

Fig. 6. Spatial Distribution of infection risk in 161 subdistricts of Wuhan. (a) Adjusted incidence rate (AIR); (b) Community safety index (CSI).

Table 4
Examination results of mediation model (n = 161). Coefficients (β) are reported, and values in brackets are t-values.

	Infection number	Population density	Infection number
Constant	1749.324 (38.677**)	843.009 (57.367**)	273.481 (-1.540)
PLAND1	−14.019 (-26.402**)	−6.563 (-38.042**)	−2.530 (-1.780)
LSI2	−2.533 (-0.899)	−0.977 (-1.068)	−0.823 (-0.353)
PLAND4	0.294 (-0.519)	−0.194 (-1.058)	0.634 (-1.353)
LPI5	−11.449 (-25.441**)	−5.417 (-37.048**)	−1.966 (-1.672)
CONTAG	−5.203 (-13.690**)	−2.142 (-17.347**)	−1.453 (-2.684**)
DIVISION	−606.769 (-6.715**)	−233.896 (-7.967**)	−197.290 (-2.222*)
SHDI	68.727 (-0.944)	−15.496 (-0.655)	95.856 (-1.593)
SHEI	548.333 (7.272**)	208.602 (8.515**)	183.136 (2.422*)
Population density			1.751 (8.498**)
n	161	161	161
R^2	0.928	0.960	0.951
Adj. R^2	0.924	0.958	0.948
F-value	70.211**	63.062**	120.364**

Note: * $p < 0.05$ ** $p < 0.01$.

3.3. Key landscape metrics

Table 7 shows the regression results in class-level models. PLAND1, LSI1, and LSI2 (t=-1.72~-3.60) in Model 1 have great impacts on AIR both globally and locally; NP2 and LSI5 (t = 2.15~2.48) are important for global AIR, while NP4 and LSI4 (t = 1.66~1.80) are more important for local AIR. This shows that cropland and woodland are good indicators for AIR while urban land and water body are better indicators for global and local AIR, respectively. PLAND1, PLAND4, LPI4, NP5, and LPI5 (t=-2.29~3.83) in Model 2 greatly influence CSI both globally and locally, while LSI4 and NP6 are important for global and local CSI, respectively. This shows that cropland, water, and urban land can be good CSI indicators. By integrating AIR and CSI, infection risk indicators at the class level were summarized. Firstly, sub-districts with less cropland and simpler cropland shape or woodland tend to have higher infection risk. Secondly, fewer water bodies, a more complex shape, and the greater advantage of larger water bodies' means higher infection risk. Finally, the more aggregated and complex the urban land is, and the less advantageous the largest urban land is, the higher the infection risk.

Table 8 shows the regression results in landscape-level models. CONTAG, DIVISION, and SHDI are negative predictors of AIR (t=-3.46~-1.71) and positive predictors of CSI (t = 1.04~2.83), while SHEI is the opposite (t=-3.08~5.86). In Models 3 and 4, CONTAG's t-values were from -3.46 to 2.83, indicating that infection risk is lower in sub-districts with good connectivity to dominant landscape classes. SHEI's t-values were from -5.14 to 5.86, suggesting that when there is no obvious dominant landscape class in a sub-district, and various patches are evenly distributed, the higher the infection risk. DIVISION's t-values were from -3.33 to 2.28, indicating that the division of various landscape patches in a sub-district is beneficial to a reduction in infection risk. SHDI's t-values were from -2.06 to 2.44, showing that the more abundant the landscape class, the lower the infection risk. Moreover, whether AIR or CSI is used to express infection risk and using whether global regression or local regression, the prediction effect of landscape-level metrics is rather stable.

3.4. Infection risk evaluation

PCA was carried out for the above sixteen indices related to infection risk. The KMO coefficient of key landscape metrics was 0.81, indicating that PCA results explained a considerable proportion of the variation (≥0.80) (Vizzari and Sigura, 2015). Table 9 shows the proportion and the cumulative proportion of the factorial components resulting from PCA. The first three axes, accounting for 73 % of variability, were selected for subsequent analysis (cut-off based on the scree plot). The first component axis (PC1, accounting for 48 % of variation) can be interpreted as a gradient of development intensity because it is directly

Table 5
Mediating effect of population density on the relationship between landscape pattern and infection risk (n = 161).

Landscape metric	Total effect (c)	a	b	Mediating effect		Direct effect (c')	Mediation
				a*b	95 % BootCI		
PLAND1	−14.019**	−6.563**	1.751**	−11.490	−1.488 ~ -0.612	−2.530	Full
LSI2	−2.533	−0.977	1.751**	−1.710	−0.041 ~ 0.004	−0.823	No
PLAND4	0.294	−0.194	1.751**	−0.340	−0.058 ~ 0.015	0.634	No
LPI5	−11.449**	−5.417**	1.751**	−9.483	−1.585 ~ -0.673	−1.966	Full
CONTAG	−5.203**	−2.142**	1.751**	−3.750	−0.376 ~ -0.148	−1.453**	Partial
DIVISION	−606.769**	−233.896**	1.751**	−409.479	−0.554 ~ -0.221	−197.290*	Partial
SHDI	68.727	−15.496	1.751**	−27.129	−0.110 ~ 0.050	95.856	No
SHEI	548.333**	208.602**	1.751**	365.197	0.164 ~ 0.392	183.136*	Partial

Note: * $p < 0.05$ ** $p < 0.01$.

Table 6
Results summary of OLS and GWR models.

Model	1−1	1−2	2−1	2−2	3−1	3−2	4−1	4−2
RSS	3868.831	3149.179	290.849	254.339	13697.723	2613.799	734.71	278.04
Sigma estimate	5.118	4.745	1.403	1.349	9.297	4.420	2.153	1.411
log-likelihood	−484.383	−467.8155	−276.057	−265.259	−586.1575	−452.815	−350.654	−272.431
AIC	1020.766	1004.106	604.114	598.993	1184.315	980.279	713.308	604.742
AICc	1031.244	1023.293	614.591	618.18	1184.86	1003.599	713.853	618.987
R^2	0.829	0.861	0.736	0.770	0.395	0.885	0.334	0.748
Adj. R^2	0.798	0.817	0.688	0.697	0.376	0.835	0.313	0.668
Best bandwidth/n	NA	161.00	NA	161.00	NA	57.65	NA	72.38

Note: RSS = residual sum of squares, NA = not applicable.

related to a higher presence and complicated shape of cropland, and dispersion and shape simplification of urban land. The second axis (PC2, accounting for 17 % of the variation) better explains the landscape level, as the aggregation, division, diversity, and richness of landscape are closely related to landscape gradient. The third axis (PC3, accounting for 8% of variation) is mainly associated with the presence and largest patch size of urban blue-green space. By observing the position of the considered variables along the structural gradient, it is possible to highlight which of them are more important for the two sub-district types (Fig. 9). As expected, infection risk in suburban sub-districts is mainly affected by urban blue-green space, while urban sub-districts are mainly affected by development intensity. Moreover, infection risk in all sub-districts can be reflected by landscape level.

On the basis that landscape pattern can indicate infection risk at the sub-district scale, community-scale infection risk can be evaluated by landscape metrics of development intensity, landscape level, and urban blue-green space. Based on the PCA results, significant landscape metrics in the GWR models were used as predictors at the community scale, and then a prediction model was developed (Fig. 10). The AIR and CSI in Fig. 11 show that urban communities are at higher risk than suburban ones, which is consistent with those sub-districts in Fig. 6. As the spatial distribution of infection risk is refined, the prediction model provides more details. For suburban areas, low-risk sub-districts may also include high-risk communities. Meanwhile, not all communities located inside one sub-district are at relatively high risk because high-risk communities may cross sub-districts despite their geographical proximity (see the upper sub-district outlined in Fig. 11). For urban areas, there are still low-risk communities in high-risk sub-districts where large-scale commercial land is concentrated because reported case numbers are relatively low in these communities with few residential areas (see the lower sub-district outlined in Fig. 11).

4. Discussion

4.1. Impact of landscape classes on infection risk

Cropland proportion accounts for less in urban districts (Fig. 2) where AIR is high and CSI is low, which explains the relationship between cropland and infectious risk. There was no evidence that grassland and bare land are related to infection risk, although they are similar to cropland in surface and plant structure. We thus considered that PLAND1 is an indicator of development intensity, as it also explains that the more complex the cropland shape, the lower the infection risk (Brant et al., 2018). Woodland proportion does not affect infection risk, which may be for two reasons. First, urban forest construction in Wuhan is so advanced that it was rated as the garden city of China in 2006. By the end of 2019, the greening rate of Wuhan reached 39.6 % (Ye and Qiu, 2021a). Second, Wuhan is a famous "City of Hundred Lakes" in China, with 166 lakes in total. Water proportion in the city reaches 1/4 of the total area (Ye and Qiu, 2021b), which further reduces the woodland ratio between sub-districts. Therefore, while there was no significant relationship between PLAND2 and infection risk, we still observed that the number and shape of forest patches were significantly related to infection risk. For LSI2 in Model 1, related research also confirmed that forest edge density and the percentage of forest-herbaceous edge are significantly associated with infection risk (Moon et al., 2019). Furthermore, researchers also found that *Salmonella typhimurium* cases are related to landscape composition (Simpson et al., 2019), especially urban land proportion and evergreen broad-leaved forest (Brant et al., 2018). Therefore, we might expect that there may be more infectious diseases related to woodland proportion. However, woodland did not significantly affect sub-district CSI, which may be because areas with more woodland are located in suburban areas where case statistic was more likely to be omitted compared to urban areas. Additionally, the COVID-19 outbreak in Wuhan occurred in winter. Wuhan is mixed evergreen and deciduous forest zone, so the prevention effect on infection risk by woodland may be weakened. Therefore, we support the view that woodland is beneficial to infection risk control, although that may vary with spatial granularity. From the Beta sign (+, −), woodland and grassland's CSI is more stable than their AIR, indicating that greening structure is very important, such as tall trees having a better protective effect than shrubs and herbs.

Similar to cropland, water proportion could also be used as a landmark indicator, although water patch number had no obvious relationship with CSI, which shows that fragmented water bodies are not conducive to infection risk. Maintaining natural water body shape

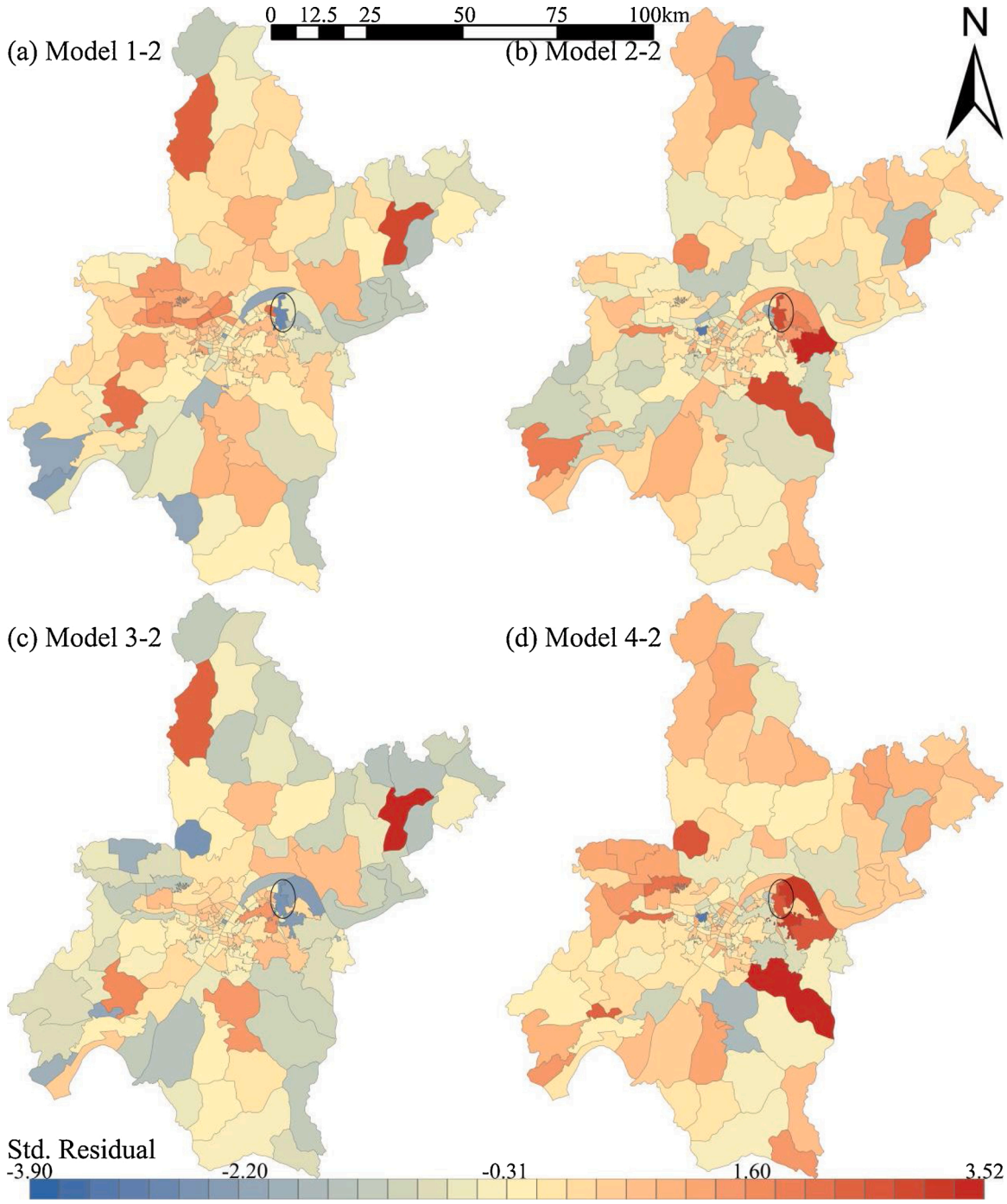

Fig. 7. Distribution of standardized residuals in geographically weighted regression models.

without further fragmentation is beneficial to infection risk prevention, and water is an important factor in the study of water-borne infectious diseases. For instance, relevant research shows that water bodies are important landscape features for determining Ross River virus infection risk (Walsh and Webb, 2018) while there is no evidence that COVID-19 transmission is associated with water (Yen et al., 2020). Moreover, the water effect on AIR is not as significant as on CSI, showing that compared with infection risk prediction in sub-districts, water bodies are more suitable as a basis for community prevention, since community safety is higher in waterfront sub-districts. In Chinese cities like Wuhan, it is generally believed that the larger the urban land LSI, the higher the urbanization level (Huang et al., 2020). We found many old communities in Wuhan's urban sub-districts (Ye and Qiu, 2020), where the ecological environment, especially land air circulation should be improved, and patch shape should not be too complex. Similarly, sub-districts with decentralized urban land layouts (larger NP5) are safer. Meanwhile, high LPI generally indicates that a sub-district may be a business district with few residential areas and therefore with fewer reported cases. Poh et al. (2020) claimed that infection risk is higher in urban areas with less woodland and more urban land because they reflect greater population aggregation. Urban land, especially buildings, usually has a large influence area near the surface wind field, which hinders airflow (Shi et al., 2019) while air quality is an important indicator of urban land use and infection risk.

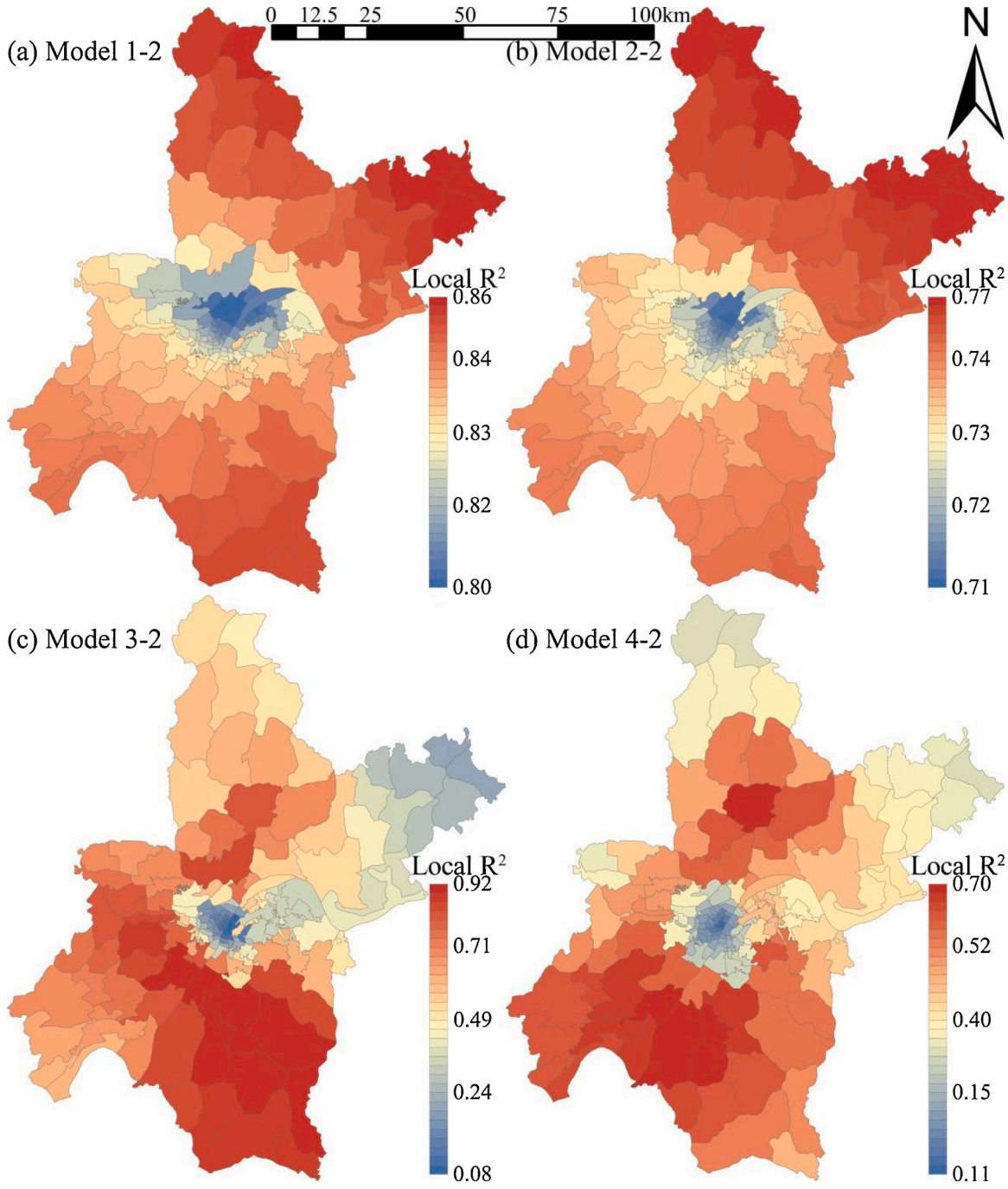

Fig. 8. Distribution of local R2 in geographically weighted regression models.

4.2. Risk evaluation and urban planning

The structure of landscape classes is also important for infectious disease spread, especially in urban sub-districts. High CONTAG indicates that a dominant landscape class with good connectivity will greatly reduce infection risk because connected urban blue-green spaces are excellent urban wind corridors (Ye and Qiu, 2021b). High DIVISION in sub-districts indicates fragmentation, and infection risk is minimal when each patch is thoroughly divided by other patches. The richer the landscape class means higher uncertainty information content (SHDI), and meanwhile, population aggregation and infection risk will be weakened where urban and ecological land are distributed separately. Low SHEI indicates a sub-district is dominated by one or a few landscape classes (especially urban land), meaning high infection risk. Although we confirm that class- and landscape-level indices are related to infection risk, the mechanism remains complex. In landscape epidemiology research, factors affecting infectious disease risk in cities can be divided into population density, mobility and connectivity, and the ecological environment (Boyce et al., 2019). These may correspond to the three principal components we extracted (construction intensity, landscape level, and urban blue-green space).

A study in U.S. metropolitan counties reported that the metropolitan population was the most significant predictor of infection rates, and that larger metropolitan areas had higher COVID-19 infection rates, because population density increases contact with other people and the likelihood of disease transmission (Hamidi et al., 2020). Our results confirm that population density has a partial mediating effect on infection number, and that development intensity is important for urban

Table 7
Estimate, Std. Err., and t-value of class-level models (Models 1 and 2).

Variable	Model 1−1			Model 1−2			Model 2−1			Model 2−2		
	Estimate	Std. Err.	t-value	Estimate	Std. Err.	t-value	Estimate	Std. Err.	t-value	Estimate	Std. Err.	t-value
Constant	56.417	7.832	7.20**	60.481	7.571	7.99**	9.099	2.147	4.24**	8.874	2.152	4.12**
PLAND1	−0.384	0.107	−3.60**	−0.360	0.109	−3.29**	0.112	0.029	3.83**	0.110	0.031	3.55**
NP1	0.057	0.070	0.81	0.065	0.072	0.90	0.004	0.019	0.20	−0.009	0.021	−0.45
LPI1	0.099	0.073	1.36	0.079	0.079	1.01	−0.030	0.020	−1.50	−0.032	0.022	−1.43
LSI1	−0.999	0.424	−2.36*	−0.766	0.444	−1.72*	0.121	0.116	1.04	0.137	0.126	1.09
PLAND2	0.090	0.222	0.40	−0.095	0.254	−0.37	0.044	0.061	0.72	0.049	0.072	0.68
NP2	0.116	0.054	2.15*	0.083	0.060	1.38	−0.023	0.015	−1.55	−0.022	0.017	−1.31
LPI2	−0.123	0.214	−0.58	0.062	0.274	0.23	0.011	0.059	0.18	0.011	0.078	0.14
LSI2	−1.522	0.485	−3.14**	−1.261	0.505	−2.50**	0.177	0.133	1.33	0.166	0.143	1.16
PLAND3	−0.178	1.244	−0.14	−0.357	1.261	−0.28	0.059	0.341	0.17	−0.005	0.358	−0.01
NP3	0.016	0.381	0.04	0.039	0.382	0.10	−0.100	0.105	−0.96	−0.063	0.108	−0.58
LPI3	0.219	1.236	0.18	0.357	1.253	0.28	−0.053	0.339	−0.16	0.013	0.356	0.04
LSI3	−0.366	0.636	−0.58	−0.418	0.661	−0.63	0.284	0.174	1.63	0.248	0.188	1.32
PLAND4	−0.012	0.146	−0.08	−0.074	0.145	−0.51	0.102	0.040	2.56**	0.104	0.041	2.54**
NP4	−0.098	0.073	−1.35	−0.127	0.076	−1.66*	0.018	0.020	0.90	0.022	0.022	1.02
LPI4	−0.016	0.125	−0.13	0.022	0.124	0.18	−0.078	0.034	−2.28*	−0.081	0.035	−2.29**
LSI4	0.841	0.461	1.83	0.890	0.496	1.80*	−0.257	0.126	−2.03*	−0.213	0.141	−1.51
PLAND5	0.078	0.101	0.77	0.021	0.097	0.22	−0.037	0.028	−1.34	−0.035	0.028	−1.25
NP5	−0.032	0.025	−1.28	−0.019	0.027	−0.70	0.014	0.007	2.06*	0.013	0.008	1.73*
LPI5	−0.065	0.065	−1.01	−0.045	0.063	−0.71	0.055	0.018	3.08**	0.055	0.018	3.04**
LSI5	0.949	0.383	2.48*	0.513	0.406	1.26	−0.171	0.105	−1.63	−0.179	0.115	−1.55
PLAND6	0.106	0.177	0.60	0.039	0.170	0.23	−0.023	0.048	−0.48	−0.025	0.048	−0.52
NP6	−0.300	0.296	−1.01	−0.294	0.303	−0.97	0.130	0.081	1.60	0.178	0.086	2.07*
LPI6	−0.103	0.179	−0.58	−0.073	0.171	−0.43	0.044	0.049	0.89	0.047	0.049	0.96
LSI6	0.988	0.760	1.30	0.774	0.784	0.99	−0.285	0.208	−1.37	−0.333	0.223	−1.49

Note: * $p < 0.05$ ** $p < 0.01$.

Table 8
Estimate, Std. Err., and t-value of landscape-level models (Models 3 and 4).

Variable	Model 3−1			Model 3−2			Model 4−1			Model 4−2		
	Estimate	Std. Err.	t-value	Estimate	Std. Err.	t-value	Estimate	Std. Err.	t-value	Estimate	Std. Err.	t-value
Constant	58.665	2.339	25.08**	56.303	4.341	26.64**	10.608	0.542	19.58**	10.679	0.740	17.01**
CONTAG	−0.123	0.036	−3.44**	−0.091	0.061	−3.46**	0.024	0.008	2.83**	0.017	0.013	2.09*
DIVISION	−27.367	8.220	−3.33**	−8.221	12.203	−2.80**	4.344	1.904	2.28*	−0.654	3.300	1.04
SHDI	−13.410	6.524	−2.06*	−3.893	10.151	−1.71*	3.693	1.511	2.44*	2.729	2.657	1.74*
SHEI	38.653	6.601	5.86**	13.812	10.324	5.04**	−7.857	1.529	−5.14**	−2.630	2.553	−3.08**

Note: * $p < 0.05$ ** $p < 0.01$.

Table 9
PCA computed from key landscape metrics identified by GWR models.

	PC1	PC2	PC3
Key landscape metrics	PLAND1, LSI1, NP5, LPI5, LSI5, NP6	CONTAG, DIVISION, SHDI, SHEI	NP2, LSI2, PLAND4, NP4, LPI4, LSI4
Definition	Development intensity	Landscape level	Urban blue-green space
Eigenvalue	7.685	2.724	1.282
Proportion explained	0.480	0.170	0.080
Cumulative proportion	0.480	0.651	0.731

sub-districts. It shows that in the city center, development intensity causes high population density, thus increasing infection risk. Secondly, it demonstrates that mobility and connectivity may matter more than population density in the spread of COVID-19 because sub-districts and communities in large cities tightly linked together through economic, social, and commuting relationships are the most vulnerable to pandemic outbreaks (Hamidi et al., 2020). In our study, landscape level represents mobility and connectivity, so it is important whether you are in an urban or suburban area because sub-districts are more likely to exchange tourists and businesspeople internally and with surrounding areas, thus increasing the risk of cross-border infections (Santos-Vega et al., 2016). Therefore, it was recommended to reduce mobility and connectivity through a closure policy in sub-districts and communities during the pandemic, which achieved good results in Wuhan. Thirdly, urban blue-green space is also important for urban infectious diseases, because water and forest not only represent geographical isolation but are also the key conduits of air circulation in cities (Santos-Vega et al., 2016), especially for the Wuhan ecological environment, which includes 11million people (Connolly et al., 2021). We found that urban blue-green space is important for suburban sub-districts that are dominated by ecological land rather than urban land, because of geographical isolation. Furthermore, suburban urban blue-green spaces are “large wedges” of the wind corridor in Wuhan, improving the ecological environment by improving air circulation (Ye and Qiu, 2021b).

Patch area and fragmentation are related to infectious disease risk (Moon et al., 2019). In sub-districts with a high proportion of natural cropland and water, the infection risk is low, and cropland and water PLAND can be used as indicators of infection risk. It is beneficial for infection risk prevention to maintain natural water body shape without further fragmentation. Wuhan defined the protection scope of 166 lakes and built a large number of wetland parks and nature reserves in 2018 (Ye and Qiu, 2021b), and rich urban blue-green spaces play a vital role in infection risk prevention. Additionally, the urban agricultural planning implemented in Wuhan from 2006 to 2020 also reserved a lot of valuable farmland as suburban areas, further reducing infection risk. Interestingly, we did not find any evidence that grassland and unused land had any impact on infection risk. In related studies, the relationship between forest land and grassland, and infection risk also showed

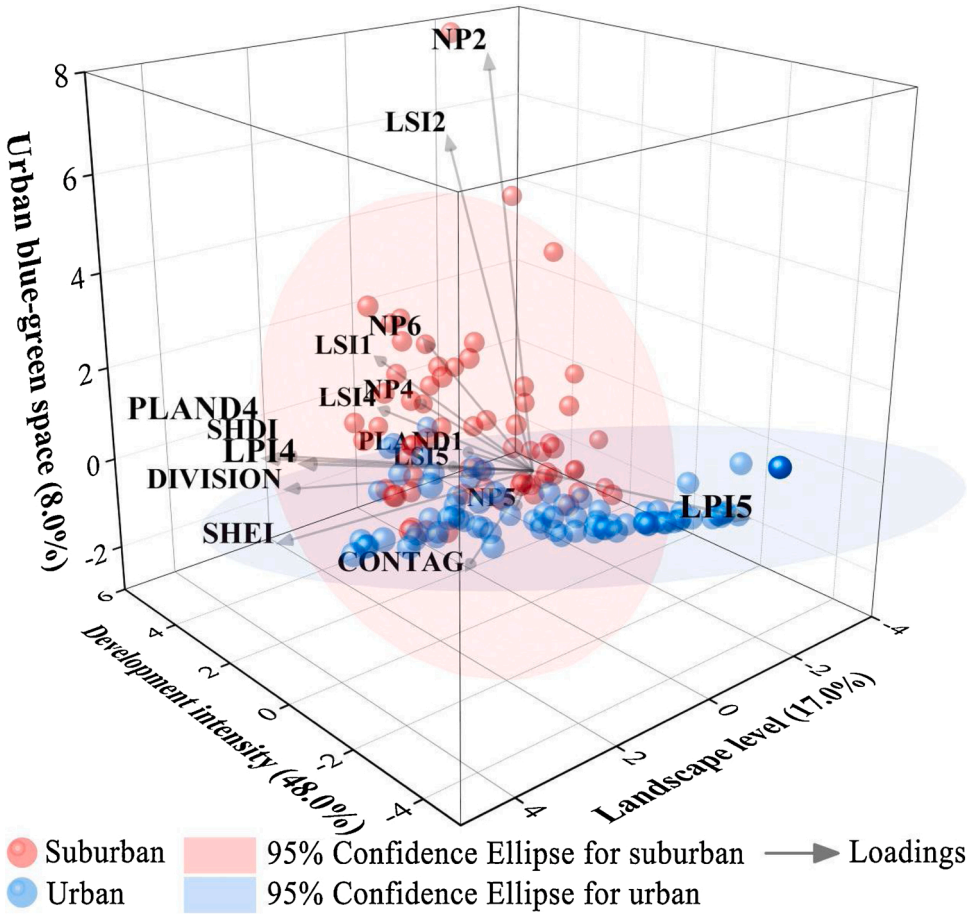

Fig. 9. Ordination biplot depicting the first three axes of PCA. The centroids of areas belonging to subdistrict classes (suburban or urban) and the standard error of their average scores are shown.

			PC1		PC2		PC3
Infection risk	=	Constant	+	Development Intensity	+	Landscape Level	+	Urban blue-green space
AIR	=	67.290	+	-0.36**PLAND1*-0.766**LSI1*	+	-0.091**CONTAG*-8.221**DIVISION*-3.893**SHDI*+13.812**SHEI*	+	-0.095**PLAND2*-1.26**LSI2*-0.127**NP4*+0.890**LSI4*
CSI	=	5.146	+	0.110**PLAND1*+0.013**NP5*+0.055**LPI5*+0.178**NP6*	+	0.017**CONTAG*+2.729**SHDI*-2.630**SHEI*	+	0.104**PLAND4*-0.081**LPI4*

Fig. 10. Prediction model of infection risk based on GWR and PCA.

differences (Moon et al., 2019). There is evidence that landscape fragmentation affects urban microclimate, which is related to infectious disease spread. As a more fragmented landscape will lead to greater urban climate change, infection risk may have a stronger relationship with landscape patterns in the fragmented and more uneven landscape, corresponding to the city center with a high development intensity (Bonnell et al., 2016).

High-risk city centers need to separate pure urban land by urban blue-green spaces to form air passages. It is unrealistic to increase cultivated land and water bodies in central urban areas, so it is pivotal to

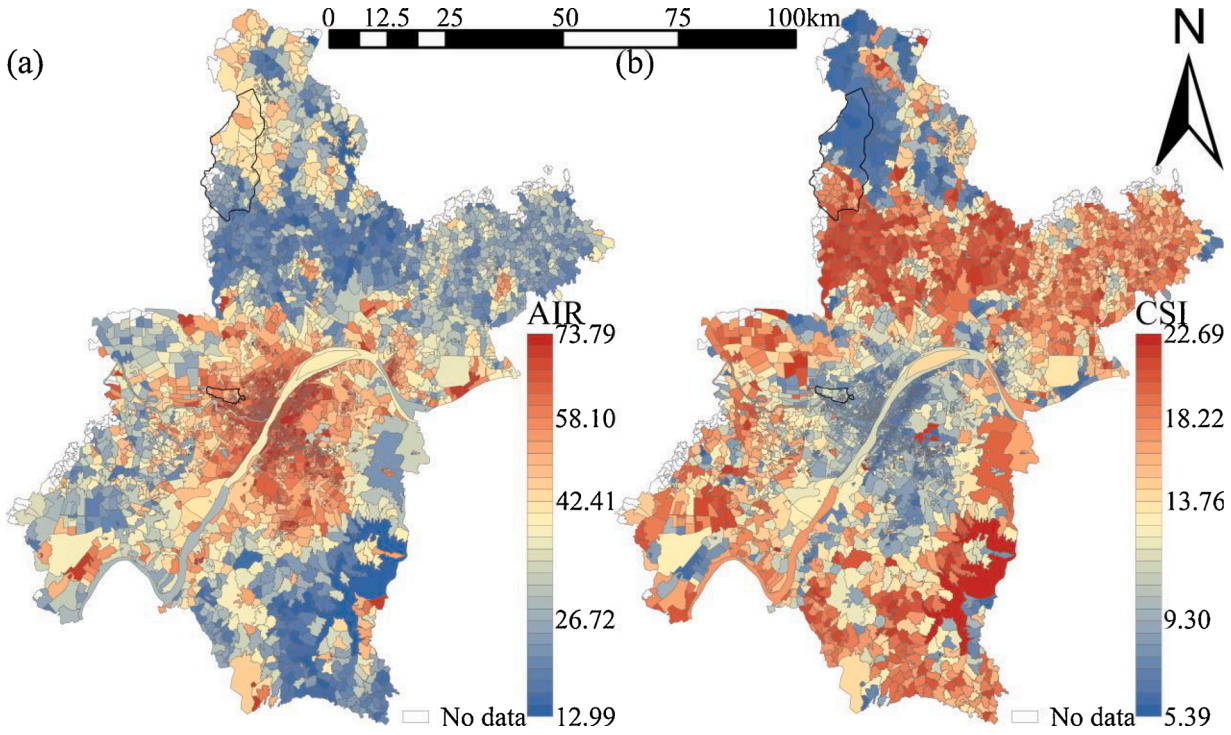

Fig. 11. Community-scale prediction of infectious risk (AIR and CSI) by class and landscape level index.

have sufficient high-level urban greening (Ye et al., 2021). In its natural state, woodland with complex shapes and a concentrated distribution has an obvious effect on infection risk prevention. For example, a centralized ecological green space with mature trees, high purity, and a close protective forest belt is ideal protection (Jim et al., 2018). In urban planning and design, great attention should be paid to the urban forests in sub-districts (Zheng et al., 2019). Urban land reduces the connectivity of ecological patches and increases infection risk. Sub-district building density may be less conducive to the ecological environment (especially air circulation) than building height. Therefore, intensive building clusters interspersed with ecological patches, like in Wuhan suburban sub-districts, are conducive to infection risk prevention. The distribution pattern of various landscape patches in sub-districts would also be conducive to infection risk reduction. Therefore, the "two ecological circles and six ecological corridors" formed in Wuhan urban planning play an important role in infection risk prevention. Furthermore, low fragmentation and large-scale natural ecological patches are important for city infection risk prevention. To deal with possible future infection risk, natural ecological patches should be preserved in suburban areas through urban planning, while in urban areas, protection of urban blue-green spaces should be increased.

4.3. Contribution to landscape epidemiology

Based on landscape epidemiology, we propose a framework to understand and evaluate infectious disease risk using urban landscape pattern, and one that has broad applicability and prospects. Firstly, this framework can apply to almost all cities with basic landscape metrics data that can be calculated on available LULC of cities, and secondly, have no scale limit as infection risk can still be evaluated even in the absence of municipal division data, although it may not be targeted for an individual sub-district or community. Generally, these findings could provide the basis for risk prevention and decision-making in sub-districts and city communities, especially in infectious disease (like COVID-19) pandemic.

Our study still had two limitations. Firstly, although we confirm the mediating role of population density on infection number and attribute it to development intensity, and that landscape pattern is an efficient indicator, there may be more factors influencing urban infection risk covered by landscape pattern. Secondly, the case number we used accounted for 1/8 of the actual case number, which may affect result accuracy. Therefore, we creatively used CSI to verify the consistence of sampling survey results when measuring AIR, which enabled us to better understand city disease infection risk.

Generally, our consistent associations across sub-districts and city communities support the relationship between landscape pattern and infection risk. Considering more comprehensive factors (e.g. urban microclimate) based on abundant multi-source data, future research could explore the specific mechanism of landscape pattern affecting urban infection risk besides population density. This will provide a more detailed policy basis for the formulation of infectious disease prevention and urban planning.

5. Conclusions

COVID-19 case numbers in 161 Wuhan sub-districts were investigated based on landscape epidemiology, and landscape metrics were calculated based on land use/land cover (LULC). Firstly, a mediation model verified a partial mediating role of population in the relationship between landscape pattern and infection number. Adjusted incidence rate (AIR) and community safety index (CSI), two indicators for infection risk in sub-districts, were 25.82~63.56 ‰ and 3.00~15.87 respectively, and central urban sub-districts had higher infection risk. Geographically weighted regression (GWR) performed better than OLS regression with AICc differences of 7.951~181.261. Adjusted R^2 in GWR models of class-level index and infection risk were 0.697 to 0.817, while those of landscape-level index were 0.668 to 0.835. Secondly, 16 key landscape metrics were identified based on GWR and used to develop a prediction model for infection risk in sub-districts and communities. From a principal component analysis (PCA), development intensity, landscape level, and urban blue-green space were determined to be the principal components affecting disease infection risk, explaining 73.1 % of the total variance. Cropland (PLAND and LSI), urban land (NP, LPI, and LSI) and unused land (NP) represent development intensity, which

greatly affects infection risk in urban areas. Landscape level CONTAG, DIVISION, SHDI, and SHEI represent mobility and connectivity, and have a profound impact on infection risk in both urban and suburban areas. Water (PLAND, NP, LPI, and LSI) and woodland (NP, and LSI) represent urban blue-green spaces, which are particularly important for infection risk in suburban areas.

Low fragmentation and natural large-scale ecological patches scale are important for infection risk prevention in cities. To deal with possible future infection risk, natural ecological patches should be preserved in suburban sub-districts through appropriate urban planning, and the protection of urban blue-green spaces should be increased in the city center. Reducing population density by limiting development intensity, weakening mobility and connectivity through closure policies, and improving the ecological environment with urban blue-green spaces (large wind corridors) are three aspects in urban planning for normal infectious disease prevention. Based on urban landscape pattern, we proposed a framework to understand and evaluate infection risk. These findings provide a basis for risk evaluation and policy-making of urban infectious disease, which is significant for community management and urban planning for infectious disease worldwide. Further research could perhaps consider more comprehensive factors and explore the impact mechanism of landscape pattern on urban infection risk to provide more specific suggestions for city epidemic prevention and urban planning.

Declaration of Competing Interest

The authors report no declarations of interest.

Acknowledgements

The present study was funded by the National Natural Science Foundation of China (Project Number 31770753). We thank Wuhan Natural Resources and Planning Information Center for the basic data provided for this study.

Appendix A. Supplementary data

Supplementary material (Table S1) related to this article can be found, in the online version, at doi:https://doi.org/10.1016/j.ufug.2021.127126.

References

Abdelsattar, A., Hassan, A.N., 2020. Assessment of malaria resurgence vulnerability in Fayoum, Egypt using remote sensing and GIS. Egyptian J. Remote Sens. Space Sci. 24 (1), 77–84. https://doi.org/10.1016/j.ejrs.2020.01.004.

Amariles, P., Ledezma-Morales, M., Salazar-Ospina, A., Hincapié-García, J.A., 2021. How to link patients with suspicious COVID-19 to health system from the community pharmacies? A route proposal. Res. Soc. Adm. Pharm. 17 (1), 1988–1989. https://doi.org/10.1016/j.sapharm.2020.03.007.

Baron, R.M., Kenny, D.A., 1986. The moderator mediator variable distinction in social psychological-research - conceptual, strategic, and statistical considerations. J. Pers. Soc. Psychol. 51 (6), 1173–1182. https://doi.org/10.1037/0022-3514.51.6.1173.

Bonnell, T.R., Ghai, R.R., Goldberg, T.L., Sengupta, R., Chapman, C.A., 2016. Spatial patterns of persistence for environmentally transmitted parasites: effects of regional climate and local landscape. Ecol. Modell. 338, 78–89. https://doi.org/10.1016/j.ecolmodel.2016.07.018.

Boyce, M.R., Katz, R., Standley, C.J., 2019. Risk factors for infectious diseases in urban environments of Sub-Saharan Africa: a systematic review and critical appraisal of evidence. Trop Med Infect Dis. 4 (4), 123. Retrieved from. https://www.mdpi.com/2414-6366/4/4/123.

Brant, T.A., Okorie, P.N., Ogunmola, O., Ojeyode, N.B., Fatunade, S.B., Davies, E., et al., 2018. Integrated risk mapping and landscape characterisation of lymphatic filariasis and loiasis in South West Nigeria. Parasite Epidemiol. Control 3 (1), 21–35. https://doi.org/10.1016/j.parepi.2017.12.001.

Camacho, A., Eames, K., Adler, A., Funk, S., Edmunds, J., 2013. Estimation of the quality of life effect of seasonal influenza infection in the UK with the internet-based Flusurvey cohort: an observational cohort study. Lancet 382, S8. https://doi.org/10.1016/S0140-6736(13)62433-2.

Connolly, C., Keil, R., Ali, S.H., 2021. Extended urbanisation and the spatialities of infectious disease: demographic change, infrastructure and governance. Urban Stud. 58 (2), 245–263. https://doi.org/10.1177/0042098020910873.

Deilami, K., Hayes, J.F., McGree, J., Goonetilleke, A., 2017. Application of landscape epidemiology to assess potential public health risk due to poor sanitation. J. Environ. Manage. 192, 124–133. https://doi.org/10.1016/j.jenvman.2017.01.051.

Dramstad, W.E., Tveit, M.S., Fjellstad, W.J., Fry, G.L.A., 2006. Relationships between visual landscape preferences and map-based indicators of landscape structure. Landsc. Urban Plan. 78 (4), 465–474. https://doi.org/10.1016/j.landurbplan.2005.12.006.

Emmanuel, N.N., Loha, N., Okolo, M.O., Ikenna, O.K., 2011. Landscape epidemiology: an emerging perspective in the mapping and modelling of disease and disease risk factors. Asian Pac. J. Trop. Dis. 1 (3), 247–250. https://doi.org/10.1016/S2222-1808(11)60041-8.

Gao, L.Q., Hethcote, H.W., 1992. Disease transmission models with density-dependent demographics. J. Math. Biol. 30 (7), 717–731. Retrieved from ://WOS:A1992JF11900004.

Halimi, M., Farajzadeh, M., Delavari, M., Takhtardeshir, A., Moradi, A., 2014. Modelling spatial relationship between climatic conditions and annual parasite incidence of malaria in southern part of Sistan & Balouchistan Province of Iran using spatial statistic models. Asian Pac. J. Trop. Dis. 4, S167–S172. https://doi.org/10.1016/S2222-1808(14)60434-5.

Hamidi, S., Sabouri, S., Ewing, R., 2020. Does density aggravate the COVID-19 pandemic? J. Am. Plan. Assoc. 86 (4), 495–509. https://doi.org/10.1080/01944363.2020.1777891.

Hassan, M.S., Bhuiyan, M.A.H., Tareq, F., Bodrud-Doza, M., Tanu, S.M., Rabbani, K.A., 2021. Relationship between COVID-19 infection rates and air pollution, geo-meteorological, and social parameters. Environ. Monit. Assess. 193 (1) https://doi.org/10.1007/s10661-020-08810-4.

Hayes, A., 2013. Introduction to Mediation, Moderation, and Conditional Process Analysis: A Regression-Based Approach.

Hoek, G., Beelen, R., de Hoogh, K., Vienneau, D., Gulliver, J., Fischer, P., Briggs, D., 2008. A review of land-use regression models to assess spatial variation of outdoor air pollution. Atmos. Environ. 42 (33), 7561–7578. https://doi.org/10.1016/j.atmosenv.2008.05.057.

Hoyle, H., Hitchmough, J., Jorgensen, A., 2017. All about the 'wow factor'? The relationships between aesthetics, restorative effect and perceived biodiversity in designed urban planting. Landsc. Urban Plan. 164, 109–123. https://doi.org/10.1016/j.landurbplan.2017.03.011.

Hu, B.S., Qiu, W.Q., Xu, C.D., Wang, J.F., 2020. Integration of a Kalman filter in the geographically weighted regression for modeling the transmission of hand, foot and mouth disease. BMC Public Health 20 (1). https://doi.org/10.1186/s12889-020-08607-7.

Huang, X., Wang, Y., Li, J., Chang, X., Cao, Y., Xie, J., Gong, J., 2020. High-resolution urban land-cover mapping and landscape analysis of the 42 major cities in China using ZY-3 satellite images. Sci. Bull. 65 (12), 1039–1048. https://doi.org/10.1016/j.scib.2020.03.003.

Jain, V.K., Kumar, S., 2015. An effective approach to track levels of Influenza-A (H1N1) pandemic in India using twitter. Procedia Comput. Sci. 70, 801–807. https://doi.org/10.1016/j.procs.2015.10.120.

Jim, C.Y., Konijnendijk van den Bosch, C., Chen, W., 2018. Acute challenges and solutions for urban forestry in compact and densifying cities. J. Urban Plan. Dev. 144. https://doi.org/10.1061/(ASCE)UP.1943-5444.0000466.

Kempen, J.H., Pistilli, M., Begum, H., Fitzgerald, T.D., Liesegang, T.L., Payal, A., et al., 2019. Remission of non-infectious anterior scleritis: incidence and predictive factors. Am. J. Ophthalmol. 223, 377–395. https://doi.org/10.1016/j.ajo.2019.03.024.

Li, J., Wang, Z., Lai, C., Wu, X., Zeng, Z., Chen, X., Lian, Y., 2018. Response of net primary production to land use and land cover change in mainland China since the late 1980s. Sci. Total Environ. 639, 237–247. https://doi.org/10.1016/j.scitotenv.2018.05.155.

Łowicki, D., 2019. Landscape pattern as an indicator of urban air pollution of particulate matter in Poland. Ecol. Indic. 97, 17–24. https://doi.org/10.1016/j.ecolind.2018.09.050.

Ma, Y., Zhao, Y., Liu, J., He, X., Wang, B., Fu, S., et al., 2020. Effects of temperature variation and humidity on the death of COVID-19 in Wuhan, China. Sci. Total Environ. 138226. https://doi.org/10.1016/j.scitotenv.2020.138226.

MacKinnon, D.P., Lockwood, C.M., Williams, J., 2004. Confidence limits for the indirect effect: distribution of the product and resampling methods. Multivariate Behav. Res. 39 (1), 99–128. https://doi.org/10.1207/s15327906mbr3901_4.

McGarigal, K., 2014. Fragstats Help. Dep. Environ. Conserv. Univ. Massachusetts, Amherst, pp. 1–182.

Messier, K.P., Jackson, L.E., White, J.L., Hilborn, E.D., 2015. Landscape risk factors for Lyme disease in the eastern broadleaf forest province of the Hudson River valley and the effect of explanatory data classification resolution. Spat. Spatiotemporal Epidemiol. 12, 9–17. https://doi.org/10.1016/j.sste.2014.10.002.

Moon, K.A., Pollak, J., Poulsen, M.N., Hirsch, A.G., DeWalle, J., Heaney, C.D., et al., 2019. Peridomestic and community-wide landscape risk factors for Lyme disease across a range of community contexts in Pennsylvania. Environ. Res. 178, 108649. https://doi.org/10.1016/j.envres.2019.108649.

Ostfeld, R.S., Glass, G.E., Keesing, F., 2005. Spatial epidemiology: an emerging (or re-emerging) discipline. Trends Ecol. Evol. 20 (6), 328–336. https://doi.org/10.1016/j.tree.2005.03.009.

Poh, K.C., Medeiros, M.C.I., Hamer, G.L., 2020. Landscape and demographic determinants of Culex infection with West Nile virus during the 2012 epidemic in Dallas County, TX. Spat. Spatiotemporal Epidemiol. 33, 100336 https://doi.org/10.1016/j.sste.2020.100336.

Santos-Vega, M., Martinez, P.P., Pascual, M., 2016. Climate forcing and infectious disease transmission in urban landscapes: integrating demographic and

socioeconomic heterogeneity. In: Rodo, X. (Ed.), Human Health in the Face of Climate Change, Vol. 1382, pp. 44–55.
Schwab-Reese, L.M., Hovdestad, W., Tonmyr, L., Fluke, J., 2018. The potential use of social media and other internet-related data and communications for child maltreatment surveillance and epidemiological research: scoping review and recommendations. Child Abuse Negl. 85, 187–201. https://doi.org/10.1016/j.chiabu.2018.01.014.
Shi, Y., Ren, C., Lau, K.K.-L., Ng, E., 2019. Investigating the influence of urban land use and landscape pattern on PM2.5 spatial variation using mobile monitoring and WUDAPT. Landsc. Urban Plan. 189, 15–26. https://doi.org/10.1016/j.landurbplan.2019.04.004.
Simpson, K.M.J., Mor, S.M., Ward, M.P., Walsh, M.G., 2019. Divergent geography of Salmonella Wangata and Salmonella Typhimurium epidemiology in New South Wales, Australia. One Health 7, 100092. https://doi.org/10.1016/j.onehlt.2019.100092.
UN-HABITAT, 2020. World Cities Report 2020. Retrieved from. https://unhabitat.org/sites/default/files/2020/10/wcr_2020_report.pdf.
Uuemaa, E., Mander, Ü., Marja, R., 2013. Trends in the use of landscape spatial metrics as landscape indicators: a review. Ecol. Indic. 28, 100–106. https://doi.org/10.1016/j.ecolind.2012.07.018.
Vinarti, R.A., Hederman, L.M., 2019. A personalized infectious disease risk prediction system. Expert Syst. Appl. 131, 266–274. https://doi.org/10.1016/j.eswa.2019.04.042.
Vizzari, M., Sigura, M., 2015. Landscape sequences along the urban–rural–natural gradient: a novel geospatial approach for identification and analysis. Landsc. Urban Plan. 140, 42–55. https://doi.org/10.1016/j.landurbplan.2015.04.001.
Walsh, M.G., Webb, C., 2018. Hydrological features and the ecological niches of mammalian hosts delineate elevated risk for Ross River virus epidemics in anthropogenic landscapes in Australia. Parasit. Vectors 11 (1), 192. https://doi.org/10.1186/s13071-018-2776-x.
Wang, K., Qi, W., 2017. Space-time relationship between urban municipal district adjustment and built-up area expansion in China. Chin. Geogr. Sci. 27 (2), 165–175. https://doi.org/10.1007/s11769-017-0856-z.
Wang, X., Ning, L., Yu, J., Xiao, R., Li, T., 2008. Changes of urban wetland landscape pattern and impacts of urbanization on wetland in Wuhan City. Chin. Geogr. Sci. 18 (1), 47–53. https://doi.org/10.1007/s11769-008-0047-z.
Wang, W., Jin, Y.Y., Yan, C., Ahan, A., Cao, M.Q., 2016. Local spatial variations analysis of smear-positive tuberculosis in Xinjiang using Geographically Weighted Regression model. BMC Public Health 16. https://doi.org/10.1186/s12889-016-3723-4.
Webster, E., 2020. Tubercular landscape: land use change and Mycobacterium in Melbourne, Australia, 1837–1900. J. Hist. Geogr. 67, 48–60. https://doi.org/10.1016/j.jhg.2019.10.009.
Ye, Y., Qiu, H., 2020. Stormwater regulation and storage by green space of drainage system: a case study of West Port Drainage System in Wuhan. Chinese Landscape Architecture 4, 55–60. https://doi.org/10.19775/j.cla.2020.04.0055.
Ye, Y., Qiu, H., 2021a. Exploring affecting factors of park use based on multisource big data: case study in Wuhan, China. J. Urban Plan. Dev. 147 (1), 05020037 https://doi.org/10.1061/(ASCE)UP.1943-5444.0000656.
Ye, Y., Qiu, H., 2021b. Environmental and social benefits, and their coupling coordination in urban wetland parks. Urban For. Urban Green 60, 127043. https://doi.org/10.1016/j.ufug.2021.127043.
Ye, Y., Qiu, H., Zhang, Q., 2021. Study on the service scope and optimized regulation of Lake Park in the Central District of Wuhan. Chinese Landscape Architecture 37 (01), 6. https://doi.org/10.19775/j.cla.2021.01.0074.
Yen, M.-Y., Schwartz, J., Chen, S.-Y., King, C.-C., Yang, G.-Y., Hsueh, P.-R., 2020. Interrupting COVID-19 transmission by implementing enhanced traffic control bundling: implications for global prevention and control efforts. J. Microbiol. Immunol. Infect. 53 (3), 377–380. https://doi.org/10.1016/j.jmii.2020.03.011.
Young, S.G., Carrel, M., Kitchen, A., Malanson, G.P., Tamerius, J., Ali, M., Kayali, G., 2017. How's the flu getting through? Landscape genetics suggests both humans and birds spread H5N1 in Egypt. Infect. Genet. Evol. 49, 293–299. https://doi.org/10.1016/j.meegid.2017.02.005.
Zhang, S.-T., Yuan, H.-Y., Duan, L.-L., 2020a. Analysis of human behavior statistics law based on WeChat Moment. Phys. A Stat. Mech. Its Appl. 540, 122854. https://doi.org/10.1016/j.physa.2019.122854.
Zhang, W., Chang, W.J., Zhu, Z.C., Hui, Z., 2020b. Landscape ecological risk assessment of Chinese coastal cities based on land use change. Appl. Geogr. 102174. https://doi.org/10.1016/j.apgeog.2020.102174.
Zheng, Y., Lan, S., Chen, W.Y., Chen, X., Xu, X., Chen, Y., Dong, J., 2019. Visual sensitivity versus ecological sensitivity: an application of GIS in urban forest park planning. Urban For. Urban Green. 41, 139–149. https://doi.org/10.1016/j.ufug.2019.03.010.
Zhou, C., Su, F., Pei, T., Zhang, A., Du, Y., Luo, B., et al., 2020. COVID-19: challenges to GIS with big data. Geogr. Sustainability 1 (1), 77–87. https://doi.org/10.1016/j.geosus.2020.03.005.
Zhu, Y., Xie, J., 2020. Association between ambient temperature and COVID-19 infection in 122 cities from China. Sci. Total Environ. 138201. https://doi.org/10.1016/j.scitotenv.2020.138201.